International Journal of Biological Macromolecules 160 (2020) 1212–1219

Contents lists available at ScienceDirect

International Journal of Biological Macromolecules

journal homepage: http://www.elsevier.com/locate/ijbiomac

Conformational activation of ribosome recycling by intra- and inter-molecular dynamics of RRF

Guangtao Song [a,1], Benjin Xu [a,b,c,1], Huigang Shi [b,d,1], Yong Zhang [a], Dejiu Zhang [a], Xintao Cao [a,b], Zengrui Liu [a,e], Ran Guo [a,e], Yan-Zhong Guan [e], Yanhui Chu [f], Xinzheng Zhang [b,d,*], Jizhong Lou [a,b,**], Yan Qin [a,b,**]

[a] Key Laboratory of RNA Biology, CAS Center for Excellence in Biomacromolecules, Institute of Biophysics, Chinese Academy of Sciences, 15 Datun Road, Chaoyang District, Beijing 100101, China
[b] University of Chinese Academy of Sciences, Beijing 100049, China
[c] Laboratory Medicine Department in Fenyang College of Shanxi Medical University, Fenyang 032200, China
[d] National Laboratory of Biomacromolecules, CAS Center for Excellence in Biomacromolecules, Institute of Biophysics, Chinese Academy of Sciences, Beijing 100101, China
[e] Department of Physiology, Mudanjiang Medical University, Mudanjiang 157011, China
[f] Heilongjiang Key Laboratory of Anti-Fibrosis Biotherapy, Mudanjiang Medical University, Mudanjiang 157011, China

ARTICLE INFO

Article history:
Received 27 March 2020
Received in revised form 21 May 2020
Accepted 27 May 2020
Available online 30 May 2020

Keywords:
Ribosome recycling factor
Molecular flexibility
Domain orientation
Molecular dynamics simulation
Single-molecule FRET
Cryo-EM

ABSTRACT

Ribosome recycling is the final step of the cyclic process of translation, where the post-termination complex (PoTC) is disassembled by the concerted action of ribosome recycling factor (RRF) and elongation factor G (EF-G) in the sub-second time range. Since, however, both the RRF and PoTC display highly dynamic action during this process, it is difficult to assess the molecular details of the interactions between the factors and the ribosome that are essential for rapid subunit separation. Here we characterized the molecular dynamics of RRF and PoTC by combined use of molecular dynamics simulations, single molecule fluorescence detection and single-particle cryo-EM analysis, with time resolutions in the sub-millisecond to minute range. We found that RRF displays two-layer dynamics: intra- and inter-molecular dynamics during ribosome splitting. The intra-molecular dynamics exhibits two different configurations of RRF: 'bent' and 'extended'. A single-site mutant of RRF increases its propensity to the 'extended' conformation and leads to a higher binding affinity of RRF to the PoTC. The inter-molecular dynamics between RRF and EF-G in the PoTC reveals that the domain IV of EF-G pushes against the domain II of RRF, triggering the disruption of the major inter-subunit bridge B2a, and catalyzes the splitting.

© 2020 Published by Elsevier B.V. All rights reserved.

1. Introduction

The protein translation is a four-step cyclic process in which the genetic information encoded in an mRNA is converted into a sequence of amino acids in a protein catalyzed by the ribosome [1–5]. When a ribosome reaches a termination codon on an mRNA, the newly synthesized polypeptide is released from the ribosome, forming a post-termination complex (PoTC). The bacteria use ribosome recycling factor (RRF) together with elongation factor G (EF-G) and GTP to disassemble the PoTC, freeing the ribosome for the next round of translation (Figs. 1A and S1) [2,6,7]. Since RRF ablation induces severe decrease of protein biosynthesis *in vivo* [8], the factor and recycling step have been regarded essential for bacterial life.

RRF is a basic protein composed of about 185 amino acids. Structures of RRF from several species reveal that it is normally composed of two domains which adopt an L-shape. Domain I, the long arm of the "L", consists of residues 1–28 and 107–185, forming three long α-helix bundles. Domain II, the short arm, consists of residues 32–102, forming a β-α-β-sheet motif (Figs. 1B and S2A) [9,10]. The two domains are connected by two highly flexible linkers and relative orientation of domain II differs substantially in various structures (Figs. 1B and S2B). An early hydroxyl radical probing study suggests that RRF binds to the ribosome complex at a well-defined location in the subunit interface cavity [11]. Cryo-electron microscopy (cryo-EM) studies of *T. thermophilus* RRF (ttRRF) bound *E. coli* ribosomes showed that RRF was in two very different positions (Fig. S2C) [12]. Studies on the kinetic mechanism for ribosome recycling revealed that ribosome splitting required EF-G binding to an already RRF-containing ribosome, resulting in a maximal recycling rate of 25 s^{-1} at the cost of about one GTP hydrolyzed per splitting event [13]. Therefore, the RRF intra- and inter-molecular dynamics may affect the functions of the ribosome and the factors during recycling. However,

* Correspondence to: X. Zhang, National Laboratory of Biomacromolecules, CAS Center for Excellence in Biomacromolecules, Institute of Biophysics, Chinese Academy of Sciences, Beijing 100101, China.
** Correspondence to: J. Lou, Y. Qin, Key Laboratory of RNA Biology, CAS Center for Excellence in Biomacromolecules, Institute of Biophysics, Chinese Academy of Sciences, 15 Datun Road, Chaoyang District, Beijing 100101, China.
E-mail addresses: xzzhang@ibp.ac.cn (X. Zhang), jlou@ibp.ac.cn (J. Lou), qiny@ibp.ac.cn (Y. Qin).
[1]These authors contributed equally to this work.

https://doi.org/10.1016/j.ijbiomac.2020.05.254
0141-8130/© 2020 Published by Elsevier B.V. All rights reserved.

2.2. Single-molecule fluorescence experiments

Single-molecule fluorescence experiments were performed with an objective-type total internal reflection fluorescence microscope. For the smFRET study on RRF dynamics experiments, Cy3/Cy5-labeled and N-terminal biotin-tagged RRFs were directly immobilized on the polyethylene glycol-passivated cover-glass surface through streptavidin–biotin interaction. For the single-molecule study of the RRF binding, purified PoTC were first immobilized *via* hybridization between its mRNA with the pre-immobilized biotinylated DNA oligonucleotides. 10 nM Alexa-488 labeled RRF was incubated in the chamber, allowing the RRF molecules to bind the surface immobilized PoTC. After 5 min of incubation, unbound RRF were washed away with the imaging buffer. Imaging was performed at room temperature in a buffer (20 mM HEPES, pH 7.8, 8.2 mM $MgSO_4$, 80 mM NH_4Cl, 100 mM KCl, 2 mM $MgCl_2$). An oxygen scavenging system (2 units μl^{-1} glucose oxidase, 20 units μl^{-1} catalase, 0.8% β-D-glucose and 2 mM Trolox (Sigma-Aldrich)) was used in all experiments to prevent the organic fluorophores from severe photo-fatigue. The time resolution for all the experiments was 100 ms. Detailed methods of smFRET data acquisition and analysis were described in previous studies [15]. The FRET efficiency of a single molecule was approximated as $FRET = I_A / (I_D + I_A)$, where I_D and I_A are the background and leakage-corrected emission intensities of the donor and acceptor, respectively. The histograms of the FRET of the RRF were obtained by averaging the first 50 frames of each FRET trace for every individual molecule after manually filtering photo-bleaching effects. For RRF binding experiments, each single-molecule trajectory was fit to a hidden Markov model with an initial guess of 2 states (Bound and release states, respectively). Time resolved population histograms of the bound state (bin size of 0.1 s) were further fitted with single exponential decay to obtain the bound lifetime of the RRF molecules.

2.3. Molecular dynamics (MD) simulations

The initial conformations of the RRF were taken from the solved structures (PDB code 3J0D (for ecRRF) and 4V9D (for ttRRF)). The model of D61R mutated ecRRF is obtained by in-silico mutation from WT ecRRF structure using the MUTATE plugin of VMD software [16]. These initial structures were solvated in rectangular TIP3P water boxes respectively (~10.6 × 7.5 × 5.7 nm^3 for ecRRF and ~11.0 × 8.1 × 5.8 nm^3 for ttRRF). Two angles θ and φ were used to describe the relative position of domain

2.5. Polysome breakdown assay

Polysome was prepared from *E. coli* MRE600 as previously described [18]. Polysome (0.2–0.6 A_{260} units) was incubated with puromycin, RRF, EF-G and GTP in 200 μl of RRF buffer (20 mM Hepes-KOH (pH 7.6), 8.2 mM $MgSO_4$, 80 mM NH_4Cl, 4 mM 2-mercaptoethanol) at 30 °C for 15 min. The sedimentation profiles of reactions were obtained using sucrose density gradient centrifugation (15–45%, w/v) sucrose in RRF buffer, Beckman SW40 rotor, 36,000 rpm, 3.5 h, 4 °C. The results were analyzed by A_{254} measurement.

2.6. Directed hydroxyl radical probing assay

The Fe(II)-RRF was prepared as described before [11]. Briefly, about 50-time amount of Fe(II)-BABE was incubated with the cysteine-containing RRF mutants at 37 °C for 30 min, and the excess reagent was then removed by ultrafiltration. This Fe(II)-RRF (10 μM) was then incubated with the PoTC (1 μM) in RRF binding buffer at 37 °C for 10 min, then on ice for 5 min. 1 μl of 250 mM ascorbic acid and 1 μl of 2.5% hydrogen peroxide were then added to 50 μl of the Fe(II)-PoTC·RRF and incubated on ice for 10 min. The reaction was stopped by adding 2.5 μl of 80 mM thiourea. The rRNA was precipitated with 0.3 M NaOAc and extracted with trizol reagent (Invitrogen). The location of 16S and 23S rRNA backbone cleavage was detected by primer extension with reverse transcriptase. Extension products were resolved by 8% urea-PAGE (8 M urea) and analyzed with a Molecular Dynamics

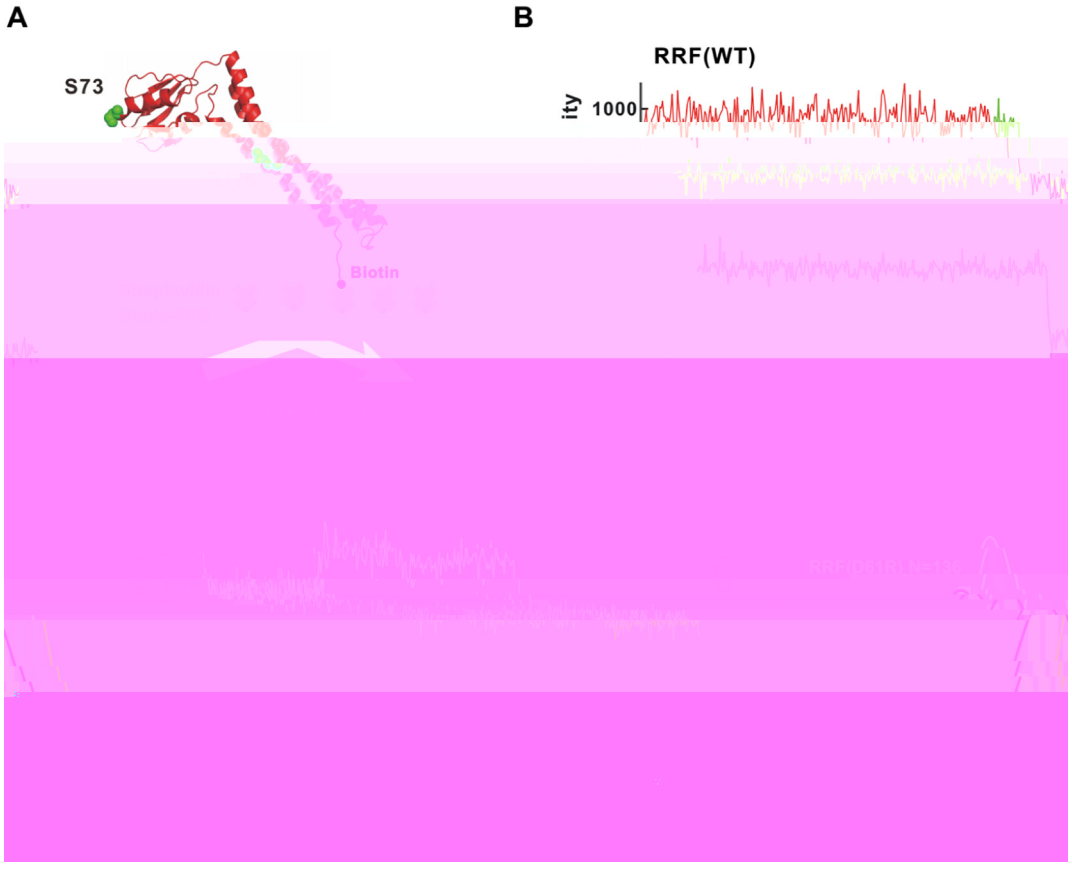

Fig. 2. smFRET study on the intra-molecular dynamics of RRF. (A) Experimental setup of the assay. (B)–(C) Typical smFRET signal traces for the ecRRF (B) and its D61R mutant (C). (D) FRET histogram of the labeled ecRRFs.

toward 50S subunit in both complexes. To certify this observation, we used directed hydroxyl radical probing of rRNA from Fe(II)-BABE modified RRF proteins bound to the PoTC [11]. RRF residues 56 and 77 were used to probe the orientation of domain II. We found that the 23S rRNA sarcin loop (helix 95) could be cleaved from both positions of RRF(WT), and much stronger cleavage was observed from D61R mutant (Fig. 4B). These results are in agreement with the cryo-EM data that the domain II of RRF(D61R) preferred to bind to the 50S subunit, similar to that of

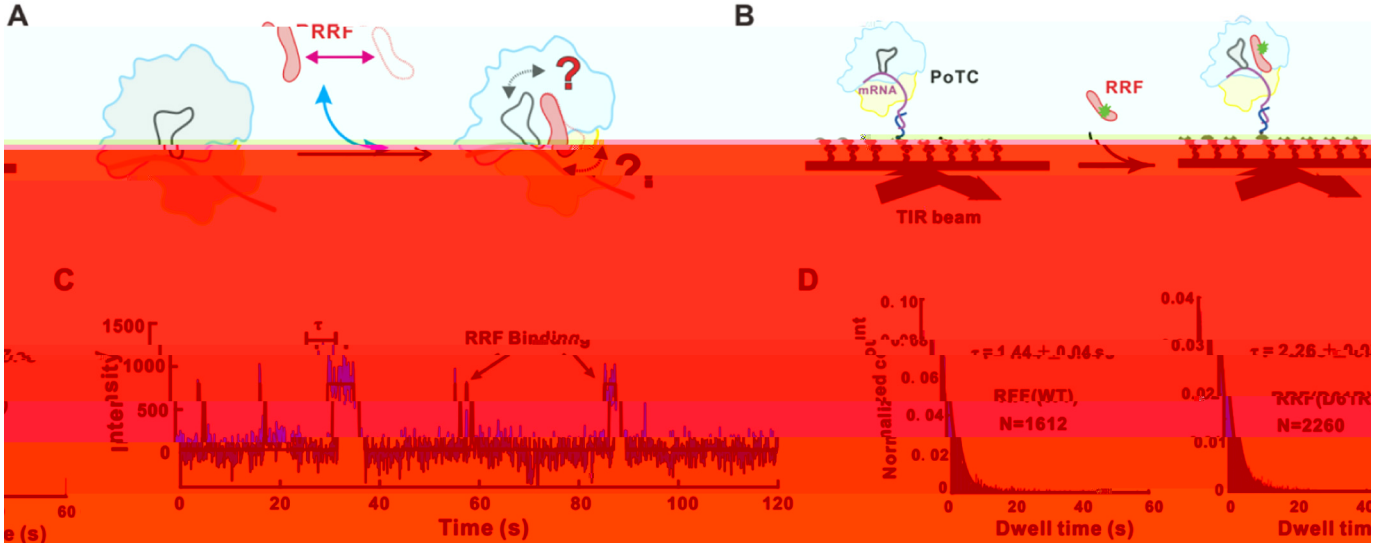

Fig. 3. Direct observation of RRF binding to PoTC. (A) Schematic model of RRF binding to PoTC and the question marks remained. (B) Experimental setup of the assay. (C) A typical single-molecule fluorescence trace, imaged at 100 millisecond time resolution at room temperature. Idealization of the fluorescence change is overlaid in red. (D) Dwell-time analysis of wild-type (WT) or D61R mutant RRF binding to PoTC.

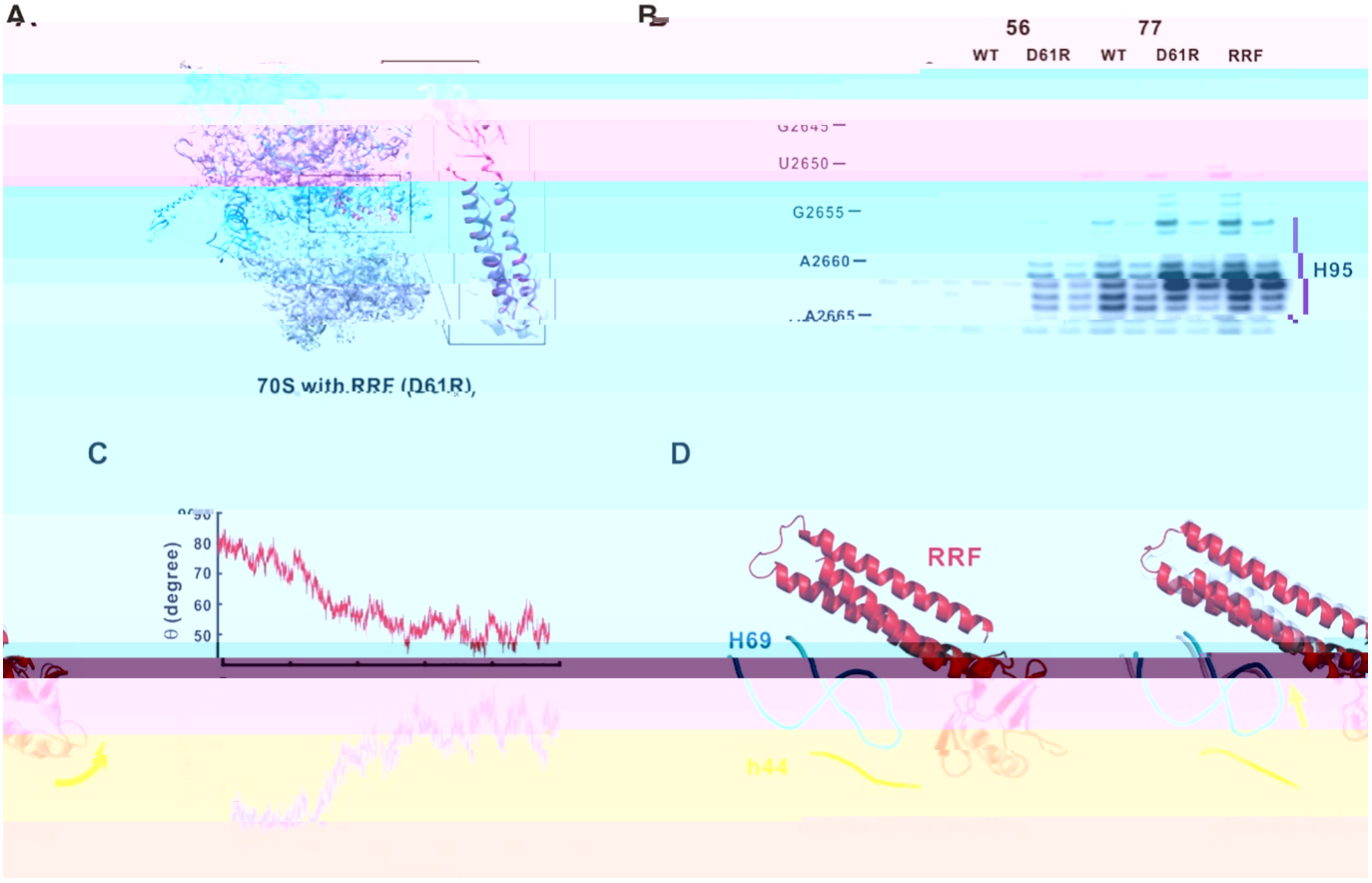

Fig. 4. Inter-molecular dynamics of RRF: conformational activation of ribosome recycling. (A) Cryo-EM map of 70S ribosome with RRF(D61R). A zoom-in view of RRF in was showed. (B) Directed hydroxyl radical probing of 23S rRNA from PoTC·RRF-Fe(II) complexes. Nucleotide numbers on the left correspond to the position of 23S rRNA. Purple vertical line on the right indicates the nucleotides bound with WT or D61R mutant RRF derivatized by Fe(II)-BABE at positions 56 and 77. (C) Conformational changes of RRF after EF-G binding in the MD simulations as observed by the shift of angles θ and φ. (D) Conformational changes of B2a bridge and RRF after EF-G binding in PoTC.

domain II of ttRRF inside the *E. coli* ribosome [12]. These results suggest that D61R mutation altered the dynamics of domain II and enhanced its binding to the ribosome complex. When we tested the activities of D61R mutant in ribosome recycling by measuring the reduction of naturally produced poly-PoTC [14], we found that the recycling activity was considerably compromised (Fig. S10). These results indicate that the binding of RRF(D61R) to the PoTC, although stronger than that of RRF(WT), prohibits the subsequent EF-G binding and ribosomal splitting. These results provide an explanation for the inhibitory effect of heterologous RRF on the recycling reaction [28,29].

3.3. Domain IV of EF-G pushes against domain II of RRF to catalyze ribosome splitting

To elucidate the molecular interactions between RRF and EF-G during ribosome splitting, we then performed MD simulations by generating a model system with the structures of RRF (PDB:4V9D) and EF-G (PDB:4V9P) into the PoTC structure (EMD: 8413) [30]. The resulting complex contained some small clashes between RRF domain II and EF-G domain IV. Considering the interdomain flexibility of the two factors, we adjusted the positions of EF-G domain IV to remove these clashes (Fig. S11A). After MD simulations, we found that the overall flexibility of the RRF in the PoTC was much lower than that of free RRF, mainly for the domain II (Fig. S11B). It was clear that domain II of RRF made several contacts with domain IV of EF-G and with ribosomal protein S12 (Fig. S11C). A ~20° rotation of domain II after EF-G binding was observed (Fig. 4C). More importantly, clear changes of the B2a inter-subunit bridge were detected (Fig. 4D): through binding of C1913 (H69, helix 69 of 23S rRNA) with Gln23 (RRF), the loop of H69 was peeled away from h44 (helix 44 of 16S rRNA) by the 5 Å movement of A1912 (H69) from G1494 (h44) (Fig. S11D). These results indicate that EF-G binding induces the rotation of RRF domain II and the binding of H69 loop to RRF domain I, which jointly trigger the disruption of the inter-subunit bridge B2a.

4. Conclusions

In summary, here we studied the dynamics of RRF and its binding to PoTC on multiple time-scales by combined use of MD simulation, smFRET, and cryo-EM techniques. We found that RRF displayed two-layer dynamics: intra- and inter-molecular dynamics during ribosome splitting. The intra-molecular dynamics exhibited two different configurations of RRF: 'bent' and 'extended'. RRF alone was not highly dynamic, its domain II preferred to adopt the 'bent' conformation which was similar to that of the RRF in PoTC. This preference came from the interaction network of residue 61 at the linker region. Single-site mutation from aspartate to arginine could alter this interaction network and led to a more flexible RRF, namely the 'extended' form. The inter-molecular dynamics showed that the extended conformation of RRF was more beneficial for its binding to the PoTC but did not result in higher splitting activity due to its spatial clashes against EF-G. Only upon the interactions with the bent RRF, EF-G could push against RRF, thus to trigger the disruption of the major inter-subunit bridge B2a, and catalyze the splitting. Based on these results and previous work,

we proposed an updated model for ribosome recycling (Fig. 5). PoTC ribosomes undergo spontaneous inter-subunit rotational movement, equilibrating between ratcheted and unratcheted states. RRF alone is relatively flexible and samples between bent (major) and extended (minor) states regulated by the interaction network in its hinge region. Binding of bent RRF to the PoTC is transient yet beneficial for the subsequent EF-G binding. Then EF-G pushes against RRF domain II to break the B2a bridge, and eventually disassembles the PoTC into the subunits. In contrast, extended RRF binds to the PoTC with higher affinity, with its domain II orientation toward 50S. However, this orientation of RRF is not compatible for the subsequent EF-G binding, and thus blocks the splitting reaction. In this model, the two layers of RRF dynamics play key roles in conformational activation of the PoTC and EF-G for subunits splitting and ribosome recycling.

Author statement

Guangtao Song: Data curation, Investigation, Methodology, Writing-Original draft preparation;
Benjin Xu: Data curation, Investigation, Methodology, Software;
Huigang Shi: Data curation, Investigation, Methodology, Software;
Yong Zhang: Data curation, Investigation, Methodology, Software;
Dejiu Zhang: Data curation, Investigation, Methodology, Software;
Xintao Cao: Data curation, Investigation, Methodology, Software;
Zengrui Liu: Data curation, Investigation;
Ran Guo: Data curation, Investigation;
Yan-Zhong Guan: Methodology, Supervision;
Yanhui Chu: Methodology, Supervision;
Xinzheng Zhang: Methodology, Supervision;
Jizhong Lou: Conceptualization, Methodology, Supervision, Writing-Reviewing and Editing;
Yan Qin: Conceptualization, Methodology, Supervision, Writing-Reviewing and Editing.

Acknowledgements

We thank Dr. L. He for technical assistance with the single-molecule FRET experiments. We thank B. Zhu, X. Huang, G. Ji, D. Fan, F. Sun, and the other staff at the Center for Biological Imaging (IBP, CAS) for their support in cryo-EM data collection. This work was supported by the National Key Research and Development Program of China (2018yfc1314400), Strategic Priority Research Programs (Category A) of the Chinese Academy of Sciences (XDA12010313), Key Research Program of Frontier Sciences, CAS (QYZDB-SSW-SMC028), and National Natural Science Foundation of China (11672317, 31222022, 31500662, 81871041 and 81371463).

Declaration of competing interest

The authors declare no competing financial interest.

Appendix A. Supplementary data

Supplementary data to this article can be found online at https://doi.org/10.1016/j.ijbiomac.2020.05.254.

References

[1] A. Korostelev, D.N. Ermolenko, H.F. Noller, Structural dynamics of the ribosome, Curr. Opin. Chem. Biol. 12 (2008) 674–683, https://doi.org/10.1016/j.cbpa.2008.08.037.
[2] T.M. Schmeing, V. Ramakrishnan, What recent ribosome structures have revealed about the mehx] 1of ribo8m osoj.translib01j.461o0205

[14] D. Zhang, K. Yan, Y. Zhang, G. Liu, X. Cao, G. Song, Q. Xie, N. Gao, Y. Qin, New insights into the enzymatic role of EF-G in ribosome recycling, Nucleic Acids Res. 43 (2015) 10525–10533, https://doi.org/10.1093/nar/gkv995.

[15] Y. Zeng, Y. Cui, Y. Zhang, Y. Zhang, M. Liang, H. Chen, J. Lan, G. Song, J. Lou, The initiation, propagation and dynamics of CRISPR-SpyCas9 R-loop complex, Nucleic Acids Res. 46 (2018) 350–361, https://doi.org/10.1093/nar/gkx1117.

[16] W. Humphrey, A. Dalke, K. Schulten, VMD: visual molecular dynamics, J. Mol. Graph. 14 (1996) 33–38, https://doi.org/10.1016/0263-7855(96)00018-5 (27-38).

[17] A. Perez, I. Marchan, D. Svozil, J. Sponer, T.E. Cheatham 3rd, C.A. Laughton, M. Orozco, Refinement of the AMBER force field for nucleic acids: improving the description of alpha/gamma conformers, Biophys. J. 92 (2007) 3817–3829, https://doi.org/10.1529/biophysj.106.097782.

[18] M. Zgarbova, F.J. Luque, J. Sponer, T.E. Cheatham 3rd, M. Otyepka, P. Jurecka, Toward improved description of DNA backbone: revisiting epsilon and zeta torsion force field parameters, J. Chem. Theory Comput. 9 (2013) 2339–2354, https://doi.org/10.1021/ct400154j.

[19] X. Li, P. Mooney, S. Zheng, C.R. Booth, M.B. Braunfeld, S. Gubbens, D.A. Agard, Y. Cheng, Electron counting and beam-induced motion correction enable near-atomic-resolution single-particle cryo-EM, Nat. Methods 10 (2013) 584–590, https://doi.org/10.1038/nmeth.2472.

[20] G. Tang, L. Peng, P.R. Baldwin, D.S. Mann, W. Jiang, I. Rees, S.J. Ludtke, EMAN2: an extensible image processing suite for electron microscopy, J. Struct. Biol. 157 (2007) 38–46, https://doi.org/10.1016/j.jsb.2006.05.009.

[21] S.H. Scheres [illegible] 2sid2(sc)-1-29245ew(sc)2sc6(Bif [illegible] 216(15)20.) [illegible] proved)-300(desc)-4524501k16.5ol